AGING

Senolysis by glutaminolysis inhibition ameliorates various age-associated disorders

Yoshikazu Johmura[1]*, Takehiro Yamanaka[1]†, Satotaka Omori[1]†, Teh-Wei Wang[1]†, Yuki Sugiura[2], Masaki Matsumoto[3]‡, Narumi Suzuki[1], Soichiro Kumamoto[1], Kiyoshi Yamaguchi[4], Seira Hatakeyama[4], Tomoyo Takami[3], Rui Yamaguchi[5], Eigo Shimizu[5], Kazutaka Ikeda[6], Nobuyuki Okahashi[6], Ryuta Mikawa[7], Makoto Suematsu[2], Makoto Arita[6,8], Masataka Sugimoto[7], Keiichi I. Nakayama[3], Yoichi Furukawa[4], Seiya Imoto[9], Makoto Nakanishi[1]*

Removal of senescent cells (senolysis) has been proposed to be beneficial for improving age-associated pathologies, but the molecular pathways for such senolytic activity have not yet emerged. Here, we identified glutaminase 1 (*GLS1*) as an essential gene for the survival of human senescent cells. The intracellular pH in senescent cells was lowered by lysosomal membrane damage, and this lowered pH induced kidney-type glutaminase (KGA) expression. The resulting enhanced glutaminolysis induced ammonia production, which neutralized the lower pH and improved survival of the senescent cells. Inhibition of KGA-dependent glutaminolysis in aged mice eliminated senescent cells specifically and ameliorated age-associated organ dysfunction. Our results suggest that senescent cells rely on glutaminolysis, and its inhibition offers a promising strategy for inducing senolysis in vivo.

Accumulation of senescent cells (SnCs) is associated with age-related pathologies (*1*, *2*), which can be alleviated by senolytic compounds (*3*–*7*). However, because of the heterogeneity of senescence in vivo, molecular targets that induce mortality in various types of SnCs have not yet been identified. To identify senolytic compounds, we developed a method for long-term culturing of human SnCs (hSnCs) of high purity (*8*) (fig. S1A). Senescent human fibroblast cell line hHCA2 induced by transient p53 activation with nutlin3a (n-Sen) showed high expression of p16, cluster of differentiation 26 (CD26), interleukin-6 (*IL-6*), and *IL-8* (fig. S1, B and C), and the purity appeared to be nearly 100%, as evidenced by senescence-associated β-galactosidase (SA–β-gal) positivity (fig. S1D). p16 expression and the SA–β-gal–positive population were higher in n-Sen hHCA2 cells than in other senescent hHCA2 cells [DNA damage-induced (d-Sen), oxidative-induced (ox-Sen), and replicative (r-Sen)] (fig. S1E). The transcriptome signature of n-Sen hHCA2 cells was similar to that of other hSnCs (fig. S1F). Immunocytochemical analysis revealed reduced lamin B1 and high-mobility group box 1 (HMGB1), which are senescent hallmarks (*9*, *10*), in all hSnCs (fig. S2).

Using n-Sen hHCA2 cells and short hairpin RNA (shRNA) libraries, we identified shRNAs that induce mortality (data S1). Among the top hits was glutaminase 1 (GLS1) (Fig. 1A and fig. S3A), the expression of which was increased in n-Sen hHCA2 cells compared with uninduced cells (fig. S3B). Protein absolute quantification analysis revealed that GLS1 expression was induced in n-Sen hHCA2 cells, among the ~100 proteins involved in metabolic regulation (Fig. 1B and data S2). Furthermore, the abundance of glutamate dehydrogenase (GDH), glutamine synthetase (GS), and excitatory amino acid transporter 3 (EAAT3) implicated in glutamine metabolism was increased in n-Sen hHCA2 and d-Sen hIMR-90 cells (fig. S3, C and D). Induction of GLS1 was also observed in d-Sen hIMR-90 cells (fig. S3D). GLS1 activity was increased in n-Sen hHCA2 cells (fig. S3E). The activation of glutaminolysis and its inhibition by BPTES [bis-2-(5-phenylacetamido-1,3,4-thiadiazol-2-yl)ethyl sulfide], an inhibitor of GLS1, in n-Sen hHCA2 cells were confirmed by isotope tracing using $^{13}C_5$, $^{15}N_2$ L-glutamine (fig. S4). GLS1 depletion (fig. S5A) and BPTES treatment (Fig. 1C and fig. S5B) showed that GLS1 was essential for the survival of n-Sen, d-Sen, r-Sen hHCA2, and oncogene-induced senescent (o-Sen) hIMR-90 cells as well as that of all other d-Sen cells tested (hIMR-90, hRPE-1, and mouse embryo fibroblasts) (fig. S5, B and C). Although glutamine metabolism is affected by culture conditions, GLS1 up-regulation and BPTES-induced mortality were independent of culture conditions in n-Sen hHCA2 cells (fig. S5, D and E). Other GLS1 inhibitors, C968 and CB-839, had similar inhibitory effects on n-Sen hHCA2 survival (fig. S5F). Overexpression of GLS1 failed to induce a senescent phenotype in uninduced hHCA2 cells (fig. S5G).

We tried to clarify the mechanism of GLS1 induction in SnCs. Kidney-type glutaminase (KGA)–type GLS1 was induced in n-Sen, d-Sen, and r-Sen hHCA2 cells (Fig. 1D and fig. S6A). The *KGA* transcript contains an AU-rich element (ARE) at the 3′ untranslated region (3′UTR) (*11*), which increases mRNA stability through HuC binding (*12*) under acidic conditions (*13*). HuC was essential for the induction of the *KGA* transcript and protein in n-Sen and r-Sen hHCA2 cells, respectively (fig. S6, B and C). The *KGA*-L transcript was stable in n-Sen hHCA2 cells but unstable in uninduced cells and HuC-depleted n-Sen hHCA2 cells (Fig. 1E and fig. S6D). HuC specifically bound to the *KGA*-L transcript (fig. S6E). HuC depletion reduced survival of n-Sen hHCA2 cells (fig. S6F). These results suggest that the induction of KGA arises from HuC-mediated stabilization of its transcript under acidic conditions in SnCs. This notion was further supported by the finding that incubation of n-Sen hHCA2 cells in alkaline medium (pH 8.5) reduced KGA expression (fig. S6G).

Glutaminolysis produces three important metabolites: α-ketoglutarate (α-KG), glutathione (GSH), and ammonia. Supplying dimethyl-α-KG (DM-α-KG) and/or GSH reduced ethyl ester (GSH-MEE) or N-acetyl-cysteine (NAC) as a source of cysteine or sulfur in culture medium failed to prevent the BPTES-induced death of n-Sen hHCA2 cells (Fig. 1F and fig. S6, H and I), although the contribution of glutaminolysis to total oxygen consumption was higher in n-Sen hHCA2 cells than in uninduced cells (figs. S6, J and K). By contrast, addition of ammonia to the medium (Fig. 1G) and incubation with alkaline medium (pH 8.5) (Fig. 1H and figs. S5F and S6, L and M) prevented the death of n-Sen hHCA2 cells caused by BPTES, C968, CB-839, or GLS1 depletion. Although glutamate is a precursor of nonessential amino acids (NEAAs), inhibition of glutaminolysis by BPTES did not affect NEAA amounts in n-Sen hHCA2 cells, suggesting that NEAAs were scavenged rather

[1]Division of Cancer Cell Biology, Institute of Medical Science, The University of Tokyo, 4-6-1 Shirokanedai, Minato-ku, Tokyo 108-8639, Japan. [2]Department of Biochemistry, Keio University School of Medicine, 35 Shinanomachi, Shinjyuku-ku, Tokyo 160-8582, Japan. [3]Department of Molecular and Cellular Biology, Medical Institute of Bioregulation, Kyushu University, 3-1-1 Maidashi, Higashi-ku, Fukuoka 812-8582, Japan. [4]Clinical Genome Research, Institute of Medical Science, The University of Tokyo, 4-6-1 Shirokanedai, Minato-ku, Tokyo 108-8639, Japan. [5]Human Genome Center, Institute of Medical Science, The University of Tokyo, 4-6-1 Shirokanedai, Minato-ku, Tokyo 108-8639, Japan. [6]RIKEN Center for Integrative Medical Sciences, Suehiro-cho, Tsurumi-ku, Yokohama, Kanagawa 230-0045, Japan. [7]Research Institute, National Center for Geriatrics and Gerontology, 7-430 Morioka-cho, Obu, Aichi 474-8511, Japan. [8]Division of Physiological Chemistry and Metabolism, Graduate School of Pharmaceutical Sciences, Keio University, Shibakoen, Minato-ku, Tokyo 105-0011, Japan. [9]Health Intelligence Center, Institute of Medical Science, The University of Tokyo, 4-6-1 Shirokanedai, Minato-ku, Tokyo 108-8639, Japan.
*Corresponding author. Email: mkt-naka@ims.u-tokyo.ac.jp (M.N.); johmuray@ims.u-tokyo.ac.jp (Y.J.) †These authors contributed equally to this work. ‡Present address: Department of Omics and Systems Biology, Niigata University Graduate School of Medical and Dental Sciences, 1-757 Asahimachi-douri, Chuo-ku, Niigata, Niigata 951-8510, Japan.

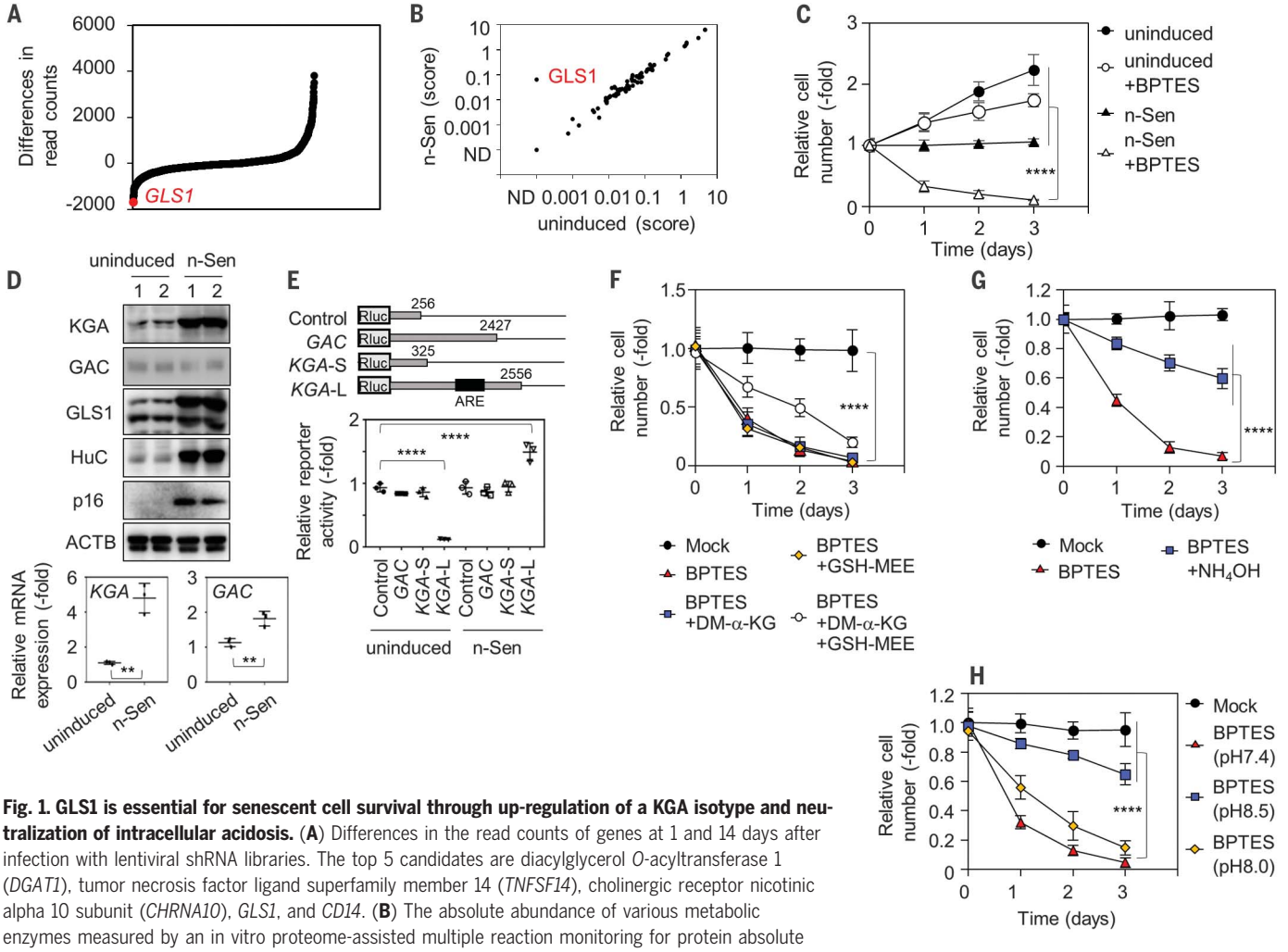

Fig. 1. GLS1 is essential for senescent cell survival through up-regulation of a KGA isotype and neutralization of intracellular acidosis. (**A**) Differences in the read counts of genes at 1 and 14 days after infection with lentiviral shRNA libraries. The top 5 candidates are diacylglycerol *O*-acyltransferase 1 (*DGAT1*), tumor necrosis factor ligand superfamily member 14 (*TNFSF14*), cholinergic receptor nicotinic alpha 10 subunit (*CHRNA10*), *GLS1*, and *CD14*. (**B**) The absolute abundance of various metabolic enzymes measured by an in vitro proteome-assisted multiple reaction monitoring for protein absolute quantification (iMPAQT) method in uninduced and n-Sen hHCA2 (n-Sen) cells. The average values of three independent samples are plotted. ND, not detected. (**C**) The relative numbers of the indicated cells in the presence or absence of BPTES (10 μM). (**D**) Immunoblotting using the indicated antibodies (top) and quantitative PCR (qPCR) using the indicated primers from the indicated cells (bottom). GAC, glutaminase C; ACTB, actin β. (**E**) Dual luciferase reporters containing the indicated 3′UTR (top) and a luciferase (luc) assay of the indicated cells expressing reporters (bottom). (**F** to **H**) The relative numbers of the indicated cells (F) in the presence or absence of BPTES (10 μM) with or without DM-α-KG (7 mM) and GSH-MEE (2 mM), (G) with or without NH_4OH (5 mM) in the presence of BPTES (10 μM), and (H) in different pH-adjusted media at the indicated times. Data are presented as means ± SD of three independent experiments. Unpaired two-tailed Student's *t* test (D) and one-way analysis of variance (ANOVA) with Dunnett's multiple comparisons post hoc test [(C) and (E) to (H)] were performed. $^{**}P < 0.01$; $^{****}P < 0.0001$.

than de novo synthesized (fig. S7A). Among amino acid transporters, only EAAT3 was highly expressed in n-Sen and d-Sen hHCA2 cells compared with uninduced cells (figs. S3, C and D, and S7B). Macropinocytosis, but not autophagy, was activated, and inhibition of macropinocytosis suppressed the survival of n-Sen hHCA2 cells (fig. S7, C and D). Supplying NEAAs in culture medium failed to prevent senescent cell death by BPTES (fig. S7E). In addition, the abundance of solute carrier family 7 member 11 (SLC7A11), the overexpression of which promotes glutaminase sensitivity, was comparable between uninduced and n-Sen hHCA2 cells (fig. S7F). Together with the finding that lowering of cysteine concentration in the medium did not alter the sensitivity of SnCs to BPTES (fig. S5D), this suggests that the mortality of SnCs after inhibition of glutaminolysis presumably occurs due to the failure in neutralizing intracellular acidosis.

Intracellular acidosis induces cell death through activation of the BCL2 and adenovirus E1B 19-kDa-interacting protein 3 (BNIP3) and mitochondrial permeability transition pore (mPTP) axis (*14*, *15*). Depletion of BNIP3 or inhibition of mPTP by decylubiquinone (DUB) or cyclosporine A (CsA) reduced the mortality of n-Sen hHCA2 cells by BPTES, C968, CB-839, or GLS1 depletion (fig. S8, A to F). Although BNIP3 colocalized with voltage-dependent anion-selective channel 1 (VDAC1), a marker of mitochondria, without BPTES (fig. S8G), in the presence of BPTES, only n-Sen hHCA2 cells showed a tight mitochondrial association with BNIP3 after alkaline treatment (fig. S8H). These data imply that mPTP activation by BNIP3 caused the cell mortality in SnCs under BPTES treatment. The amount of mitochondria-bound BNIP3 was specifically reduced in n-Sen hHCA2 cells cultured under pH 8.5 (fig. S8I). Overexpression of dominant-negative BNIP3 lacking a transmembrane domain (BNIP3-ΔTM) protected n-Sen hHCA2 cells from death after BPTES treatment or GLS1 depletion (fig. S8, J to M). BPTES-induced mortality of n-Sen hHCA2 cells was not affected by treatment with benzyloxycarbonyl-Val-Ala-Asp(OMe)-fluoromethylketone (Z-VAD-FMK), ferrostatin-1, or Nec1s (fig. S8N). The amount

of ammonium production in n-Sen hHCA2 cells and medium was high in the presence of DUB and dropped after treatment with BPTES, C968, CB-839, or GLS1 depletion (fig. S9, A to C), resulting in a lowering of the intracellular pH.

Insoluble macromolecules in lysosomes cause lysosomal membrane damage, resulting in leaking intralysosomal H^+ and subsequent intracellular acidosis (*16*). Many foci of galectin-3, a marker of membrane damage, colocalized with lysosomal-associated membrane

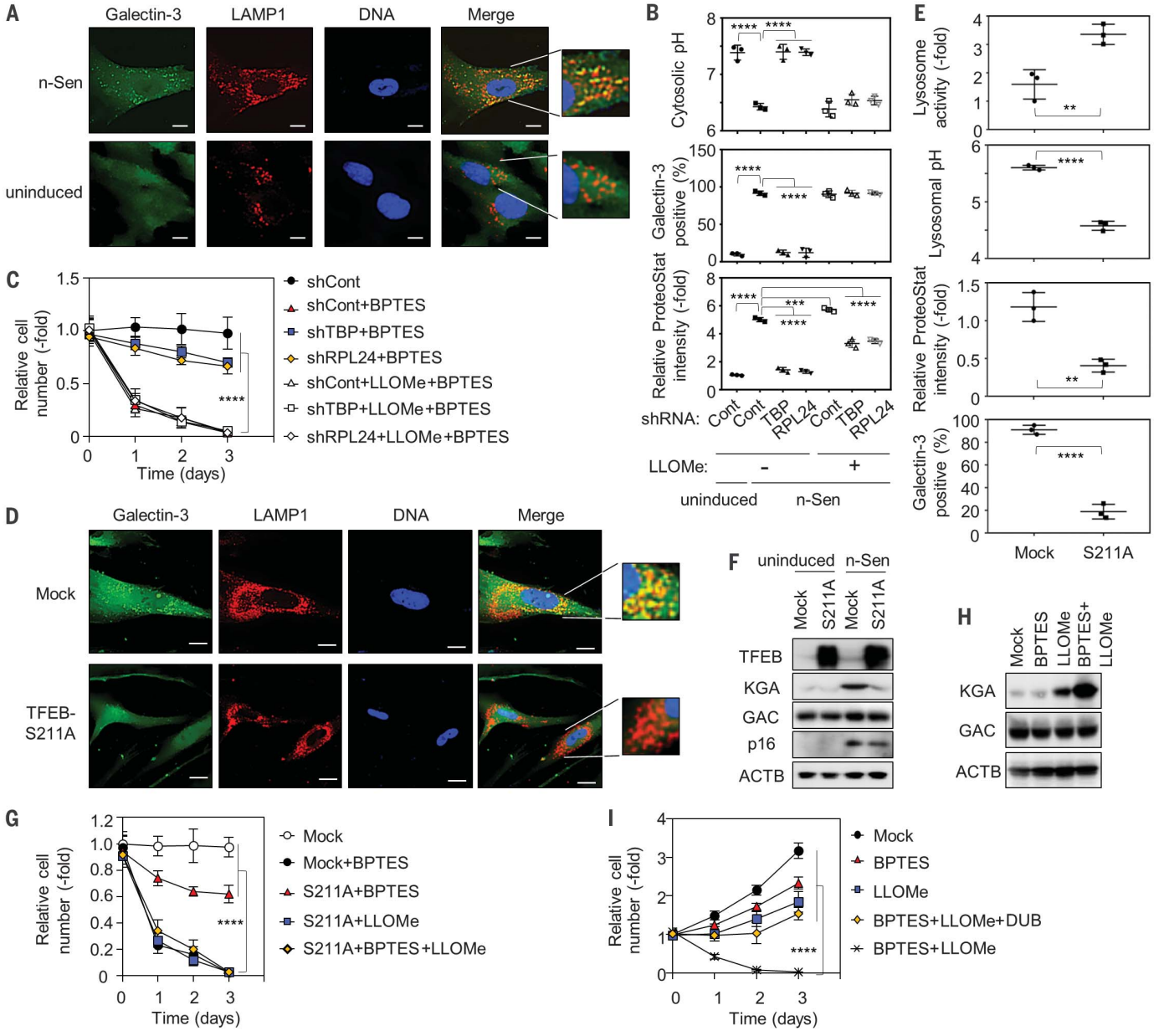

Fig. 2. Protein aggregates cause lysosomal membrane damage that provokes intracellular acidosis in SnCs. (**A**) Immunostaining of uninduced and n-Sen hHCA2, using anti–galectin-3 (green) and anti-LAMP1 (red) antibodies and Hoechst 33342 (DNA, blue). Magnified images show the colocalization between galectin-3 and LAMP1 foci. Scale bars, 20 μm. (**B**) The cytosolic pH, relative population of galectin-3–positive cells (cells with more than five galectin-3–positive foci colocalized with LAMP1: n = 200), and ProteoStat intensity of n-Sen hHCA2 cells expressing the indicated shRNA with or without LLOMe (1 mM). Cont, control. (**C**) The relative number of n-Sen hHCA2 cells expressing the indicated doxycycline (Dox)–inducible shRNA with Dox (1 μg/ml) with or without BPTES (10 μM) and LLOMe (1 mM) at the indicated times. (**D**) Immunostaining of n-Sen hHCA2 cells expressing mock or TFEB-S211A, as described in (A). Scale bars, 20 μm. (**E**) Lysosomal activity, the lysosomal pH, the ProteoStat signal, and the relative population of galectin-3–positive cells (n = 200) among the indicated n-Sen hHCA2 cells. (**F**) Immunoblotting of uninduced and n-Sen hHCA2 cells expressing mock or TFEB-S211A using the indicated antibodies. (**G**) The relative number of n-Sen hHCA2 cells expressing mock or TFEB-S211A with or without BPTES (10 μM) and LLOMe (1 mM) at the indicated times. (**H**) Immunoblotting of uninduced hHCA2 cells with or without LLOMe (1 mM and/or BPTES (10 μM) for 2 hours using the indicated antibodies. (**I**) The relative number of uninduced hHCA2 cells with or without BPTES (10 μM), LLOMe (1 mM), and/or DUB (100 μM) at the indicated times. Data are presented as means ± SD of three independent experiments. Unpaired two-tailed Student's t test (E) and one-way ANOVA with Dunnett's multiple comparisons post hoc test [(B), (C), (G), and (I)] were performed. $^{**}P < 0.01$; $^{***}P < 0.001$; $^{****}P < 0.0001$.

protein 1 (LAMP1), a marker of lysosomes, in n-Sen hHCA2 cells but not in uninduced cells (Fig. 2A). The lysosomal pH was higher in n-Sen hHCA2 cells, suggesting leaking of intralysosomal H^+ to the cytosol (fig. S10A). ProteoStat staining revealed the presence of many aggregates in lysosomes of n-Sen hHCA2 cells (fig. S10B). Amounts of endoplasmic reticulum stress markers—C/EBP homologous protein (CHOP), activating transcription factor 4 (ATF4), and ATF6—were not different between n-Sen and uninduced hHCA2 cells (fig. S10, C and D). mRNA and protein syntheses were higher in d-Sen and r-Sen hHCA2 cells than in uninduced cells (fig. S10, E and F). Suppression of RNA or protein syntheses by depletion of TATA-box binding protein 1 (TBP1) (*17*) or ribosomal protein L24 (RPL24) (*18*), respectively, reduced protein aggregates, ameliorated lysosomal membrane damage, ameliorated the extent of intracellular acidosis, and improved the survival of n-Sen hHCA2 cells in the presence of BPTES (Fig. 2, B and C, and fig. S10, F and G). Artificial lysosomal membrane damage by L-leucyl-L-leucine methyl ester (LLOMe) treatment, which induced galectin-3 foci and intracellular acidosis in uninduced hHCA2 cells when applied alone or combined with BPTES (fig. S10H), reversed the effects of TBP1 and RPL24 depletion (Fig. 2, B and C). However, mechanisms underlying high rates of RNA and protein syntheses in SnCs remain elusive.

Overexpressing constitutively active transcription factor EB (TFEB-S211A) (*19*), which promoted the expression of lysosome biogenesis-related genes (fig. S11A), reduced the levels of galectin-3 foci, protein aggregates, and intralysosomal pH and increased lysosomal activity in n-Sen hHCA2 cells (Fig. 2, D and E). Induction of KGA, stabilization of the *KGA* transcript, intracellular acidosis, and cell mortality in BPTES-treated n-Sen hHCA2 cells were suppressed by TFEB-S211A expression (Fig. 2, F and G, and fig. S11, B to D). The increased survival of cells expressing TFEB-S211A with BPTES was reversed by LLOMe treatment and by incubation with acidic medium (pH 6.2) (Fig. 2G and fig. S11E). Even in uninduced hHCA2 cells, lysosomal membrane damage by LLOMe induced KGA expression and increased mortality in the presence of BPTES (Fig. 2, H and I). The induction of KGA by LLOMe was reduced under an alkaline condition (pH 8.5), whereas incubation with acidic medium (pH 6.2) increased KGA expression in uninduced hHCA2 cells (fig. S11F).

Using comprehensive RNA sequencing (RNA-seq) data of human skin fibroblasts (*20*), we found that the amount of the *KGA* transcript was correlated with aging (Fig. 3A). As reported previously (*21*), a high expression of CD26 was observed in senescent hHCA2 cells induced by all stimuli tested (fig. S12, A to C). The CD26-positive population in lung mesenchymal cells

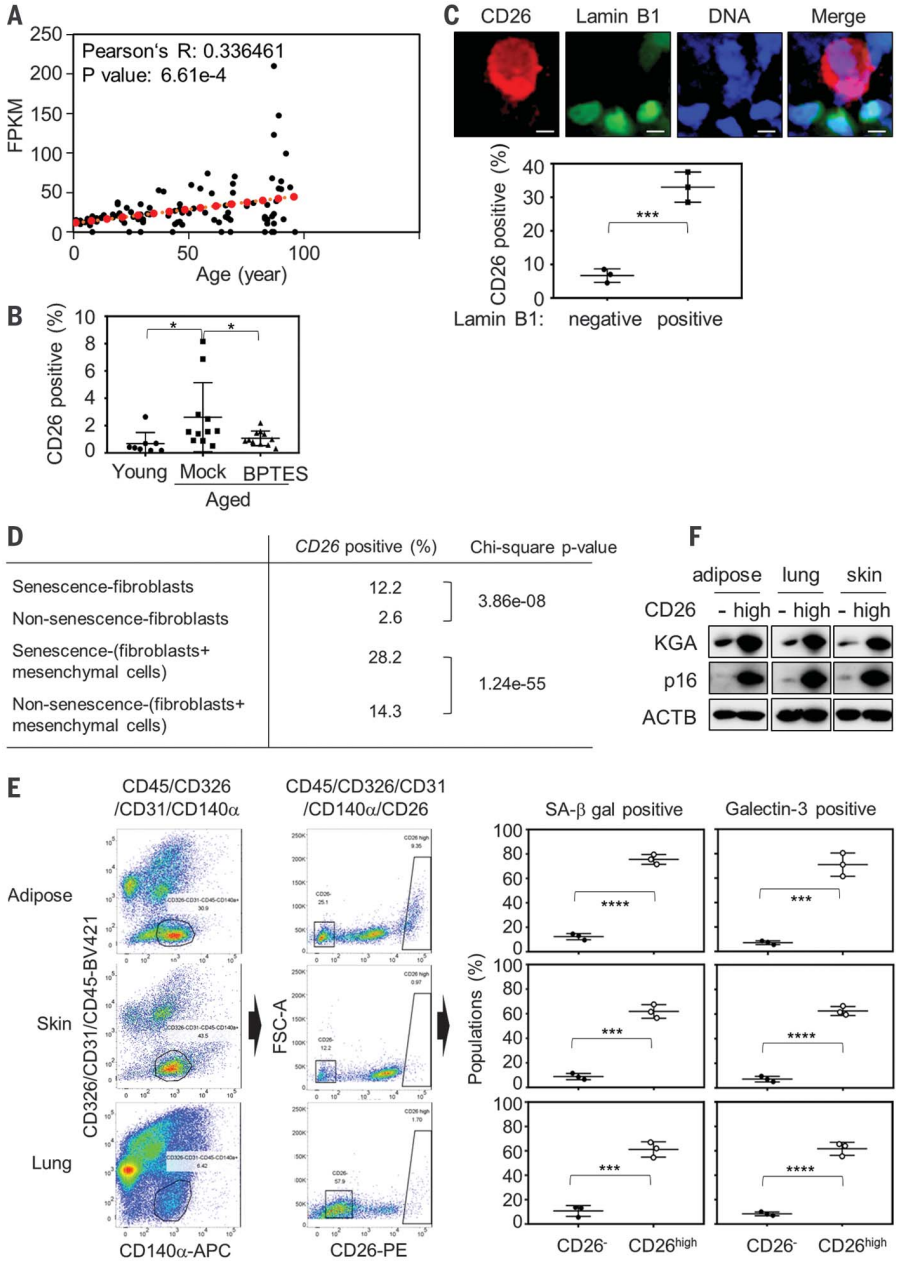

Fig. 3. GLS1 is highly expressed in in vivo SnCs from adipose tissue, skin, and lung. (**A**) Dots for each individual showing the *KGA* fragments per kilobase of exon per million reads mapped (FPKM) value from published RNA-seq data for human dermal fibroblasts versus true age (men; $n = 99$), with a line of best fit overlaid. The Pearson's correlation coefficient (R) value and P value are shown. (**B**) Relative populations of CD26-positive lung mesenchymal populations from young (12-week-old C57BL/6 male) ($n = 8$) and aged (80-week-old C57BL/6 male) mice with ($n = 11$) or without ($n = 11$) BPTES. Smirnov-Grubbs test indicated no outlier in the samples. (**C**) In situ immunostaining of intra-abdominal adipose tissues from 96-week-old aged mice ($n = 3$) with the indicated antibodies and Hoechst 33342 (DNA) (top) and the CD26-positive cell population in lamin B1–positive and –negative cells ($n = 200$ per each animal, bottom). Scale bars, 10 μm. (**D**) Single-cell RNA-seq analysis of the CD26-positive population in mouse fibroblasts with or without mesenchymal cells. (**E**) Anti-CD26 FACS of mouse mesenchymal populations ($CD45^-CD326^-CD31^-CD140\alpha^+$) and CD26-negative or CD26-high cells from the indicated tissues. The relative populations of SA–β-gal–positive cells and galectin-3–positive cells ($n = 200$ per each animal, total three animals) in the indicated population are shown. (**F**) Immunoblotting of CD26-high (high) and CD26-negative (–) mouse cells using the indicated antibodies. Data are presented as means ± SD of three independent experiments. Unpaired two-tailed Student's t test [(C) and (E)] and two-way ANOVA with a Fisher's least significant difference test (B) were performed. *$P < 0.05$; ***$P < 0.001$; ****$P < 0.0001$.

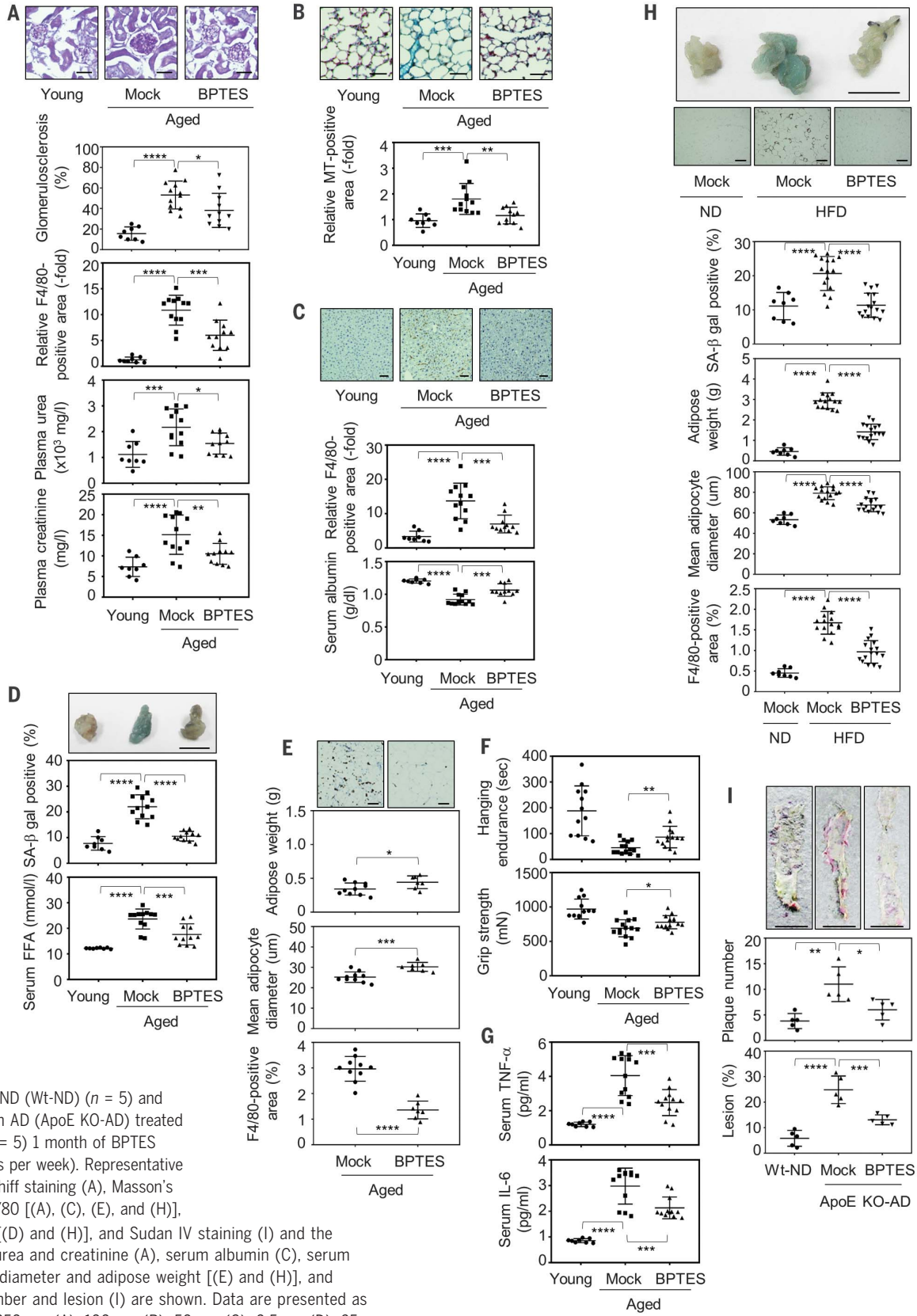

Fig. 4. BPTES treatment ameliorates age- and senescence-associated organ dysfunctions by eliminating SnCs in vivo. (**A** to **D**) Kidney (A), lung (B), liver (C), and adipose (D) tissue from 12-week-old (young) (n = 8) and 80-week-old (aged) C57BL/6 male mice with (n = 12) or without (n = 11) 1 month of repeated BPTES injection (three doses per week). (**E**) Intra-abdominal adipose tissues from 100-week-old C57BL/6 male (aged) mice with (n = 7) or without (n = 10) BPTES. (**F**) Quantification of hanging endurance (top) and grip strength (bottom) from 12-week-old (young) (n = 12) and 100-week-old (aged) C57BL/6 male mice with (n = 14) or without (n = 14) BPTES. (**G**) Quantification of serum tumor necrosis factor–α (TNF-α) (top) and IL-6 (bottom) from 12-week-old (young) (n = 8) and 80-week-old (aged) C57BL/6 male mice with (n = 12) or without (n = 11) BPTES. (**H**) Intra-abdominal adipose tissues from 48-week-old C57BL/6 male mice fed a normal diet (ND) (n = 4) or HFD for 8 weeks with (n = 8) or without (n = 8) BPTES. (**I**) Thoracic aorta from 16-week-old C57BL/6 male wild-type mice fed a ND (Wt-ND) (n = 5) and ApoE knockout mice fed an AD (ApoE KO-AD) treated with (n = 5) or without (n = 5) 1 month of BPTES administration (three doses per week). Representative images of periodic acid Schiff staining (A), Masson's trichrome staining (B), F4/80 [(A), (C), (E), and (H)], SA–β-gal staining in situ [(D) and (H)], and Sudan IV staining (I) and the quantification of plasma urea and creatinine (A), serum albumin (C), serum FFA (D), mean adipocyte diameter and adipose weight [(E) and (H)], and thoracic aorta plaque number and lesion (I) are shown. Data are presented as means ± SD. Scale bars, 250 μm (A), 100 μm (B), 50 μm (C), 0.5 cm (D), 25 μm (E), 0.5 cm [(H), top], 200 μm [(H), bottom], and 500 μm (I). Unpaired two-tailed Student's t test (E) and one-way ANOVA with Dunnett's multiple comparisons post hoc test [(A) to (D) and (F) to (I)] were performed. *P < 0.05; **P < 0.01; ***P < 0.001; ****P < 0.0001.

was higher in aged mice than in young mice and was reduced after 1 month of BPTES injection (Fig. 3B). More than 30% of lamin B1–negative cells were CD26-positive in aged mouse adipose tissues (Fig. 3C). Using a comprehensive single-cell RNA-seq dataset (*22*), SnCs were defined as *p21*-positive, *Lmnb1*-negative, and *IL-6*–positive because reads of *p16* were extremely low and could not be distinguished from those of alternate reading frame protein (ARF), excluding the possibility of using *p16* as a senescent marker for single-cell analysis. Higher proportions of senescent mouse fibroblasts and mesenchymal cells were CD26-positive as compared with nonsenescent cells (Fig. 3D). Fluorescence-activated cell sorting (FACS) using a mesenchymal population ($CD45^-CD326^-CD31^-CD140a^+$) of adipose, skin, and lung from 80-week-old mice revealed that 1 to 10% of cells were CD26-positive (Fig. 3E). The mouse CD26-high population had a higher proportion of SA–β-gal–positive cells, more galectin-3–positive cells, and higher expression of KGA and p16 than did the CD26-negative population (Fig. 3, E and F), suggesting that SnCs predominantly expressed KGA in vivo through lysosomal membrane damage-mediated acidosis. *p16* and *p21* were commonly upregulated CDK inhibitor genes in CD26-positive mouse SnCs from all the organs tested (fig. S12D). Senescence-associated secretory phenotype patterns varied among mouse CD26-positive SnCs from these organs (fig. S12E), consistent with previous reports (*23*).

We examined the effects of BPTES administration in aged mice (80-week-old males) on organ dysfunction. BPTES administration ameliorated age-associated glomerulosclerosis, macrophage invasion in kidney, and kidney dysfunction, which was reflected by abnormal levels of plasma creatinine and urea (Fig. 4A). As with a NADPH oxidase 4 inhibitor or with combining dasatinib and quercetin (*24*, *25*), BPTES administration improved lung fibrosis, macrophage invasion in the liver, and serum albumin concentration (Fig. 4, B and C). Senescence of adipogenic progenitor cells and the subsequent atrophy and macrophage infiltration in adipose tissue are features of natural aging (*26*, *27*). BPTES treatment eliminated the SA–β-gal–positive population and improved serum free fatty acids (FFAs) in the aged mice (Fig. 4D). It alleviated adipose tissue atrophy and macrophage invasion in adipose tissue in aged mice (100-week-old males) (Fig. 4E). Additionally, BPTES treatment improved age-associated weakness of grip strength and short hanging endurance as well as cytokinemia (Fig. 4, F and G). Consistent with the pathophysiological improvement of aging phenotypes, BPTES reduced the expression of *p16*, *KGA*, and *IL-6* transcripts and KGA protein in all tissues tested (fig. S13, A to F). Elimination of SnCs in vivo was confirmed by a reduction in lamin B1–negative populations in adipose tissue from the aged mice (100-week-old males) (fig. S13G).

Targeting SnCs with senolytic drugs was reported to alleviate obesity-induced disorders (*28*, *29*). High-fat diet (HFD)–induced adipocyte hypertrophy, increased SA–β-gal–positive population, and macrophage invasion in adipose tissue were improved by 1 month of BPTES injection in obese mice (48-week-old mice on HFD) (Fig. 4H), accompanied by an increase in the lamin B1–positive population and a reduction in the expression of *IL-6*, *KGA*, and *p16* (fig. S14A). BPTES treatment also improved glucose tolerance and insulin sensitivity in the obese mice (fig. S14B). Atherosclerosis of thoracic aorta in apolipoprotein E (ApoE) knockout mice (16-week-old mice) fed an atherogenic diet (AD) was alleviated by BPTES treatment with a reduced plaque numbers and lesions, accompanied by reduction in the expression of *p16*, *KGA*, and *IL-6* in abdominal aorta of the same mice (Fig. 4I and fig. S14C). In a nonalcoholic steatohepatitis model (16-week-old males), BPTES treatment also improved liver function, showing reduced concentrations of serum hydroxyproline and aspartate aminotransferase (fig. S14D). However, BPTES injection also modestly suppressed the rate of dorsal skin wound healing in mice (8-week-old males) (fig. S14E) (*30*). Overall, in addition to the clearance of SnCs, protection from senescence improved age- and senescence-associated pathogenesis.

Dysregulation of lysosomes had been proposed to be one of the senescent hallmarks. Mechanisms controlling both the quality and quantity of proteins play a pivotal role in the regulation of aging in vivo and in vitro, but precisely how the accumulation of unfolded proteins causes aging phenotypes both in cells and in the body remains enigmatic. Our results provide insights into the mechanisms underlying the relationship between protein quality control and aging in vivo. We developed a strategy for senolysis targeting a specific metabolic feature of SnCs. Elimination of SnCs and protection from senescence by inhibition of glutaminolysis in the aged body may ameliorate tissue microinflammation, prevent age-associated disorders, and even extend life span and rejuvenate an aging individual.

REFERENCES AND NOTES

1. B. G. Childs, M. Durik, D. J. Baker, J. M. van Deursen, *Nat. Med.* **21**, 1424–1435 (2015).
2. S. He, N. E. Sharpless, *Cell* **169**, 1000–1011 (2017).
3. M. Xu *et al.*, *Nat. Med.* **24**, 1246–1256 (2018).
4. M. P. Baar *et al.*, *Cell* **169**, 132–147.e16 (2017).
5. J. Chang *et al.*, *Nat. Med.* **22**, 78–83 (2016).
6. J. N. Justice *et al.*, *EBioMedicine* **40**, 554–563 (2019).
7. R. Yosef *et al.*, *Nat. Commun.* **7**, 11190 (2016).
8. Y. Johmura *et al.*, *Mol. Cell* **55**, 73–84 (2014).
9. A. R. Davalos *et al.*, *J. Cell Biol.* **201**, 613–629 (2013).
10. A. Freund, R. M. Laberge, M. Demaria, J. Campisi, *Mol. Biol. Cell* **23**, 2066–2075 (2012).
11. H. Ibrahim, Y. J. Lee, N. P. Curthoys, *Kidney Int.* **73**, 11–18 (2008).
12. G. Ince-Dunn *et al.*, *Neuron* **75**, 1067–1080 (2012).
13. J. M. Schroeder, H. Ibrahim, L. Taylor, N. P. Curthoys, *Am. J. Physiol. Renal Physiol.* **290**, F733–F740 (2006).
14. C. Vande Velde *et al.*, *Mol. Cell. Biol.* **20**, 5454–5468 (2000).
15. L. A. Kubasiak, O. M. Hernandez, N. H. Bishopric, K. A. Webster, *Proc. Natl. Acad. Sci. U.S.A.* **99**, 12825–12830 (2002).
16. M. L. Skowyra, P. H. Schlesinger, T. V. Naismith, P. I. Hanson, *Science* **360**, eaar5078 (2018).
17. P. Kotsantis *et al.*, *Nat. Commun.* **7**, 13087 (2016).
18. R. A. J. Signer, J. A. Magee, A. Salic, S. J. Morrison, *Nature* **509**, 49–54 (2014).
19. G. Napolitano, A. Ballabio, *J. Cell Sci.* **129**, 2475–2481 (2016).
20. J. G. Fleischer *et al.*, *Genome Biol.* **19**, 221 (2018).
21. K. M. Kim *et al.*, *Genes Dev.* **31**, 1529–1534 (2017).
22. Tabula Muris Consortium, *Nature* **583**, 590–595 (2020).
23. C. D. Wiley *et al.*, *Cell Metab.* **23**, 303–314 (2016).
24. L. Hecker *et al.*, *Sci. Transl. Med.* **6**, 231ra47 (2014).
25. M. Ogrodnik *et al.*, *Nat. Commun.* **8**, 15691 (2017).
26. D. J. Baker *et al.*, *Nature* **530**, 184–189 (2016).
27. M. De Cecco *et al.*, *Nature* **566**, 73–78 (2019).
28. A. K. Palmer *et al.*, *Aging Cell* **18**, e12950 (2019).
29. B. G. Childs *et al.*, *Science* **354**, 472–477 (2016).
30. M. Demaria *et al.*, *Dev. Cell* **31**, 722–733 (2014).

ACKNOWLEDGMENTS

We are grateful to A.-B. Shyu and S. A. Stewart for reagents and to C. Konishi, T. Ando, and T. Kanai for technical assistance. **Funding:** This study was supported by MEXT/JSPS KAKENHI under grant numbers JP26250027 (M.N.), JP22118003 (M.N.), JP16K15239 (M.N.), JP18H05026m (Y.J.), JP16H06148 (Y.J.), and JP16K15238 (Y.J.) and by AMED under grant numbers JP17cm0106122 (M.N.), JP17fk0310111 (M.N.), JP17gm5010001 (M.N.), and JP19gm5010003 (Y.S.), as well as by Ono Medical Research Foundation (M.N.), Princess Takamatsu Cancer Research Fund (M.N.), and Relay for Life Japan Cancer Society (M.N.). **Author contributions:** M.N. and Y.J. conceived the idea of the project; Y.J., T.Y., T.-W.W., Y.S., M.M., K.Y., R.Y., M.Sug., K.I.N., Y.F., S.I., and M.N. planned the experiments; Y.J., S.O., T.-W.W., Y.S., M.M., T.Y., N.S., S.K., K.Y., S.H., T.T., R.Y., E.S., K.I., N.O., R.M., M.Sue., and M.Sug. performed the experiments; Y.J., T.Y., T.-W.W., Y.S., M.M., K.Y., U.Y., M.Sue., M.Sug., M.A., K.I.N., Y.F., S.I., and M.N. analyzed the results; and M.N. and Y.J. wrote the manuscript with editing by all the other authors. **Competing interests:** M.N. and Y.J. are co-inventors on provisional patent application serial no. PCT/JP2019/043570: "Method for removing senescent cell, and method for preparing senescent cell." Y.J. is a shareholder and S.O. is a shareholder and CEO of Elixir Biotechnologies. All other co-authors declare that they have no competing interests. **Data and materials availability:** shRNA screening and RNA-seq data have been deposited in the Gene Expression Omnibus (GEO) under accession numbers GSE145414 and GSE138508, respectively. In vitro proteome-assisted multiple reaction monitoring for protein absolute quantification (iMPAQT) data have been deposited in the Japan Proteome Standard Repository (jPOSTrepo) under accession number JPST000730. All other data needed to evaluate the conclusions in the paper are presented in the paper and/or the supplementary materials. All materials are available from the corresponding authors.

SUPPLEMENTARY MATERIALS

science.sciencemag.org/content/371/6526/265/suppl/DC1
Materials and Methods
Figs. S1 to S14
Tables S1 to S3
References (*31*–*45*)
MDAR Reproducibility Checklist
Data S1 and S2

View/request a protocol for this paper from *Bio-protocol*.

5 March 2020; resubmitted 14 September 2020
Accepted 13 November 2020
10.1126/science.abb5916

Science

Senolysis by glutaminolysis inhibition ameliorates various age-associated disorders

Yoshikazu Johmura, Takehiro Yamanaka, Satotaka Omori, Teh-Wei Wang, Yuki Sugiura, Masaki Matsumoto, Narumi Suzuki, Soichiro Kumamoto, Kiyoshi Yamaguchi, Seira Hatakeyama, Tomoyo Takami, Rui Yamaguchi, Eigo Shimizu, Kazutaka Ikeda, Nobuyuki Okahashi, Ryuta Mikawa, Makoto Suematsu, Makoto Arita, Masataka Sugimoto, Keiichi I. Nakayama, Yoichi Furukawa, Seiya Imoto and Makoto Nakanishi

Science **371** (6526), 265-270.
DOI: 10.1126/science.abb5916

Selective destruction of senescent cells

Senescent cells are associated with a variety of age-related medical conditions and thus have been proposed as potential targets for therapy, but we do not yet have a full understanding of the underlying mechanisms. Johmura *et al.* used RNA interference to screen for enzymes essential to the survival of senescent cells (see the Perspective by Pan and Locasale). The authors identified a key role for glutamine metabolism, particularly the enzyme glutaminase 1, and demonstrated that inhibition of this pathway induced the death of senescent cells. Glutaminase targeting also ameliorated aging-related organ dysfunction and obesity-related disorders in mouse models, suggesting the potential therapeutic value of this approach.

Science, this issue p. 265; see also p. 234